The Development of TLM Models for Nonlinear Optics

Vijay Janyani[1], Ana Vukovic[1], John D. Paul[1], P. Sewell[1], T. M. Benson[1]

Abstract – **A review of techniques for modelling dispersive and nonlinear materials using the TLM method is presented. The materials are those commonly used in optics, although the methodology is directly transferable to microwave and lower frequencies. It is shown that use of the Duffing model for devices exhibiting both nonlinear and dispersive nature provides more physically meaningful results than those of a simple Kerr model.**

Keywords – **dispersive, nonlinear, optics, nonlinear switches and limiters**

I. INTRODUCTION

The behaviour of optical waves in nonlinear and dispersive materials has been the subject of intense investigations in recent years [1], driven by applications such as switching and bistability, optical limiting, pulse shaping, wavelength conversion and soliton propagation [2-5]. Time domain numerical analysis is widely used in electromagnetic modelling and seems well-suited to performing the complex simulations required by photonics devices based on nonlinear dispersive effects [6-8]. In this paper we develop models of various complexity for modelling dispersive and nonlinear dielectrics within the Transmission Line Modelling (TLM) [9] method. The models are developed, investigated and applied in one-dimension (1D), but can be extended to the three-dimensional (3D) case.

II. LINEAR DISPERSIVE DIELECTRICS

The propagation of signals in a linearly dispersive, absorptive medium is of significant interest in acoustics, wave propagation in plasma and dielectric media and in optical waveguides [10]. In this section, we develop a TLM model for a material with Lorentzian susceptibility. A Lorentzian material shows both normal and anomalous dispersion in the susceptibility. In TLM, open-circuit, short-circuit and matched stubs connected at nodes can be used to represent various material properties [9]. We represent the Lorentzian behaviour of the material susceptibility by using lumped components connected at the TLM nodes in the form of open-circuited, short-circuited and matched stubs, as shown in Fig.1. To confirm that the susceptibility behaviour obtained is indeed Lorentzian, we note that the Laplace transform of the equivalent capacitance $C_{eq}(s)$ represented by this circuit is:

$$C_{eq}(s) = \frac{C}{s^2 LC + sRC + 1} \tag{1}$$

Therefore, if Δl is the TLM cell size and $\chi_e(s)$ is the material susceptibility, $C_{eq}(s) = \varepsilon_0 \chi_e(s) \Delta l$ in TLM,

or

$$\chi_e(s) = \frac{C_{eq}(s)}{\varepsilon_o \Delta l} \tag{2}$$

or

$$\chi_e(s) = \frac{1/(L\varepsilon_0 \Delta l)}{s^2 + sR/L + 1/(LC)} \tag{3}$$

which represents a Lorentz material susceptibility, with the following equivalences:

$$\begin{aligned} C &= \Delta\chi_e \varepsilon_0 \Delta l \\ L &= \frac{1}{\omega_0^2 \Delta\chi_e \varepsilon_0 \Delta l} \\ R &= 2\delta L \end{aligned} \tag{4}$$

where $\Delta\chi_e$ is the susceptibility contrast, ω_0 is the resonant frequency and δ is the damping frequency of the Lorentzian material. These L, C and R values can be simulated in TLM using a series combination of a short-circuit stub, an open-circuit stub and a matched stub at the nodes.

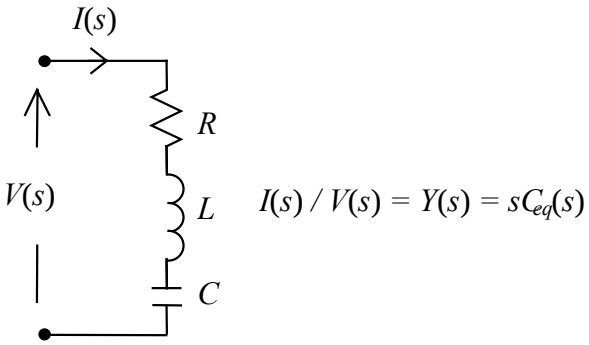

Fig.1. An equivalent circuit representation of Lorentzian susceptibility in TLM

Using the above model, we simulate a Gaussian pulse propagation in a Lorentz material, and the results obtained are compared with those obtained using a Z-transform technique

[1] Authors are from George Green Institute for Electromagnetics Research, University of Nottingham, Nottingham NG7 2RD, UK. Email:ana.vukovic@nottingham.ac.uk

[7]. The material properties are chosen as $\Delta\chi_e$ = 1.435, ω_0 = 2π x 20 x 10^9rads^{-1}, $\delta = 10^{-6}\omega_0$ as in [7]. The results obtained are shown in Fig.2 and clearly demonstrate the pulse broadening associated with material dispersion. These results are in precise agreement with those reported in [7].

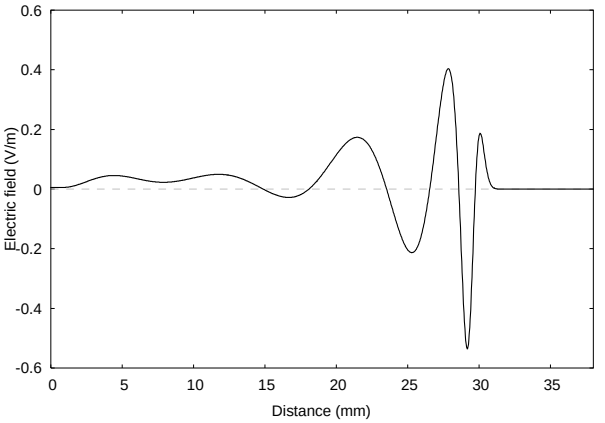

(a)

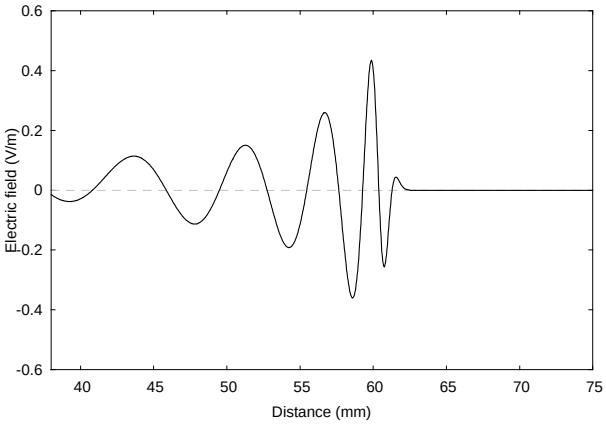

(b)

Fig.2. Electric field in the Lorentz material after (a) 0.1 *ns*, and (b) 0.2 *ns*

III. DOUBLE RESONANCE LORENTZ MODEL DIELECTRIC

The modelling principles developed in section II are now extended to a multi-Lorentz material, i.e. one in which the susceptibility shows more than one resonant feature. The complex refractive index in this case is given by:

$$n(\omega) = \left(1 + \frac{b_0^2}{\omega^2 + \omega_0^2 + 2j\delta_0\omega} + \frac{b_1^2}{\omega^2 + \omega_1^2 + 2j\delta_1\omega}\right) \qquad (5)$$

where ω is the frequency, ω_0 and ω_1 are the resonant frequencies, δ_0 and δ_1 are the damping frequencies, and b_0 and b_1 are constants given by the product of square of the resonant frequency and the static susceptibility. Representative material parameters are taken as those for a typical fluoride-type glass with visible and infrared resonance lines [10] of ω_0= 1.7414 x 10^{14} rads^{-1} and ω_1= 9.1448 x 10^{15} rads^{-1}. The frequency

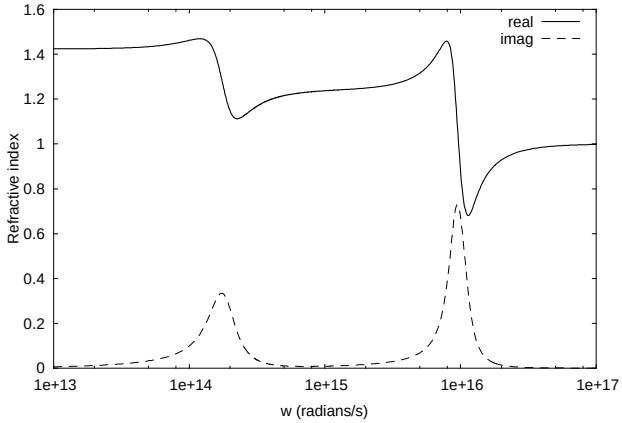

Fig.3. Dispersion of the real and imaginary parts of the refractive index for a typical Fluoride-type glass

dispersion of the real and imaginary parts of the complex refractive index is shown in Fig. 3.

The response of the material to a Heaviside step function-modulated sine wave excitation was simulated, as in [10]. A TLM cell size of 10^{-8}m was used throughout. The time evolution of field profiles at various positions in the material are presented in Fig.4(a) for a signal angular frequency ω = 1.2 x 10^{14} rads^{-1}, which lies below the first resonance frequency in the anomalous dispersion region, and in Fig.4(b)-(d) for ω = 3 x 10^{14} rads^{-1} which lies just above the lower absorption band, near the lower end of the medium passband. All figures show the appearance of precursors, Brillouin and Sommerfield [10], before the propagating signal. Fig.4(b,c,d) shows how the precursors evolve along the distance and eventually dominate the signal, which in turn reduces in amplitude, as is typical for the above dispersive material. The results show excellent agreement with those obtained using a hybrid numerical-asymptotic code for the dispersive pulse calculations [10].

IV. KERR MODEL FOR NONLINEAR DIELECTRIC

In this section, a nonlinear frequency-independent dielectric susceptibility is modelled using the TLM method. The stub technique originally proposed in [11] is used, in which the nonlinearity is included in the model by updating the material properties at each time step. The nonlinearity considered is of Kerr type, i.e. the refractive index of the material varies with the instantaneous local intensity according to the relation:

$$n = n_0 + n_2 I \qquad (6)$$

where n is the total refractive index of the material, n_0 is the linear refractive index, n_2 is the nonlinearity coefficient and I is the local intensity of signal.

In order to show the effectiveness and application of the method, a grating consisting of alternate layers of high and low linear index n_0 of 2 ± 0.05 is analysed. Each layer is $\lambda_m/4$ thick, where λ_m is the wavelength of the signal of frequency f_0 (taken here to be 300 THz) in a material whose linear

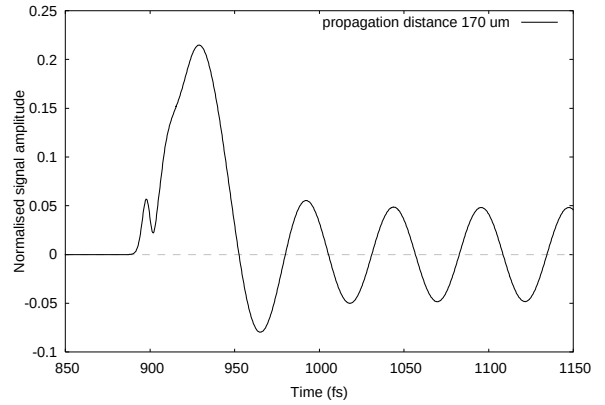

(a)

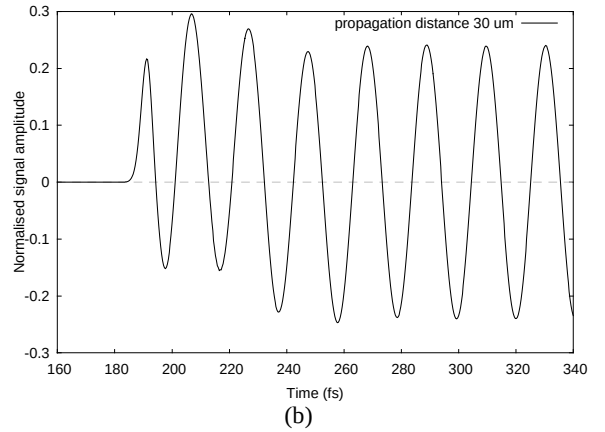

(b)

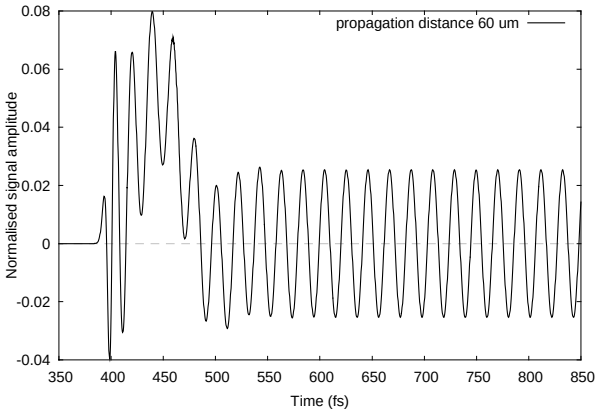

(c)

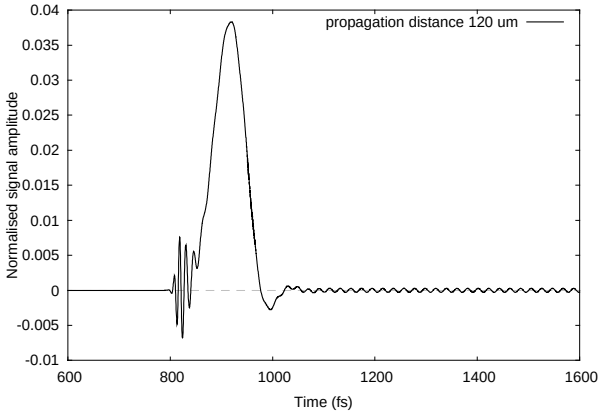

(d)

Fig.4. Field profile in a double-resonance Lorentz-model dielectric for a signal frequency of (a) ω of 1.2 x 10^{14} rads^{-1}, and (b), (c), (d) field profile for ω of 3 x 10^{14} rads^{-1}

refractive index is 2. Such a structure is expected to have a transmission stopband, which is centred at the Bragg frequency f_0, and whose width and sharpness depend on the linear index contrast and the total number of layers in the grating [2]. A positive Kerr nonlinearity is introduced in all the layers, i.e. n_2 is always positive. The value of n_2 is fixed at 0.001 in normalised units reciprocal to those of I, which is, in turn, normalised to units of V^2.

The introduction of the Kerr nonlinearity into the structure has the effect of dynamically shifting the stopband with the level of the applied signal. Since the average refractive index of the material now increases with the intensity, an instantaneous shift in the stopband towards lower frequencies is expected with increasing intensity. If the signal is located in the stopband suitably close to the stopband-passband border, then this may give rise to self-switching and bistability in the nonlinear grating [5]. We explore this switching and bistability behaviour in the present section and observe the effect of (i) the number of layers in the grating, (ii) the frequency of the applied signal and (iii) the magnitude of the nonlinearity coefficient on the switching behaviour of the grating.

In the simulations, a continuous sine wave is launched from free space as an excitation. For a given combination of the number of layers in the structure and nonlinearity coefficient, the signal frequency is chosen to lie towards the higher frequency end of the linear stopband. The applied signal intensity is gradually increased from a low to a high value. For each step of intensity, the output time history at a point in free space on the far end of the grating is recorded, and then, using an FFT, the intensity of this output signal at the desired frequency is determined. In this way a curve is plotted showing the output intensity as a function of input signal intensity (Figure 5(a)). It is observed from this curve that for low input intensity, the signal is still in the stopband, and the output intensity (i.e. the transmittance) is low. With increasing input intensity, the stopband starts to move and eventually the signal is placed in the passband thus giving rise to a switching action, with transmittance close to unity and the device turned ON.

These devices exhibit bistable operation, in which a single input intensity gives two different output intensities (transmittances). This can be seen on the hysteresis curve of Fig.5(b). The hysteresis curve is obtained in a single TLM run starting from small input intensities when the signal frequency is still in the stopband. The input intensity is gradually increased in steps until the device is driven well into the ON state. The input intensity is then decreased in the same steps until the device reaches well within the OFF state. It is observed that the curve now traces out a hysteresis loop, Fig.5(b).

Fig.5(c) shows that for signal frequencies which lie close to the top edge of the linear stopband, the switching is achieved for relatively lower signal intensities, and the width of the hysteresis curve obtained is smaller. Fig.5(d) suggests that for a fewer number of layers in the grating, the jump in the output intensity after the grating switches ON takes place for higher input intensity. This behaviour reflects the observation that the linear stopband is expected to be less sharp in this case.

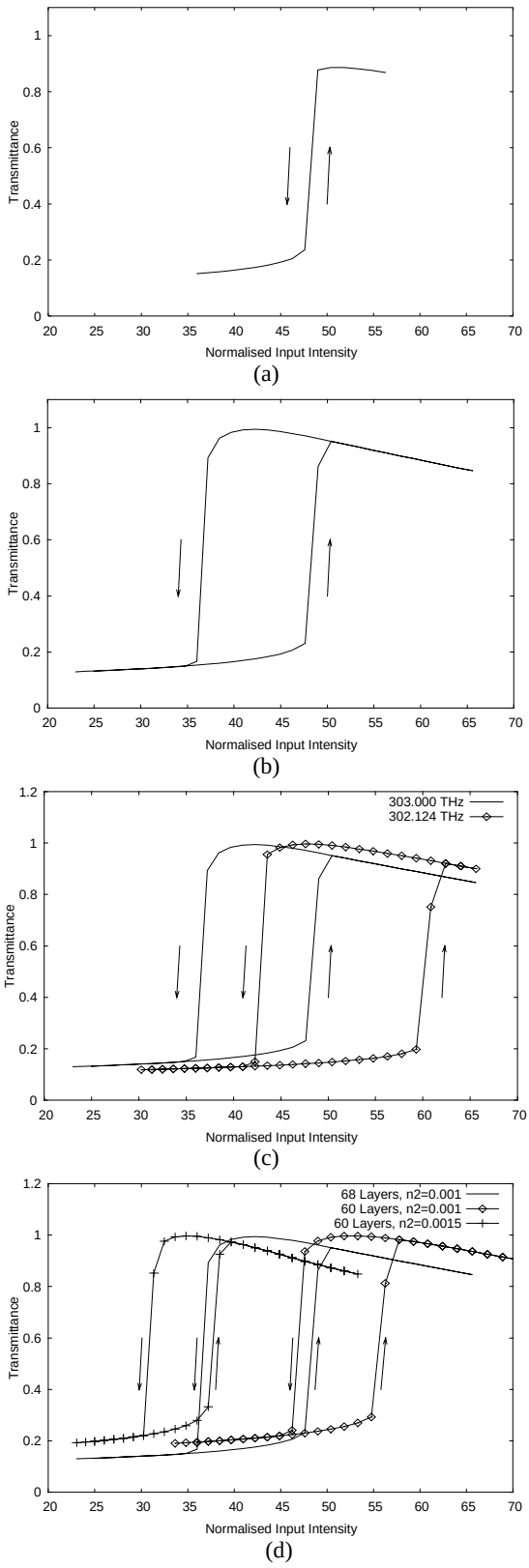

Fig.5. Characteristics of a nonlinear grating, (a) switching, (b) bistable behaviour, (c) the effect of the frequency of the applied signal on the switching action, and (d) the effect of number of layers and the nonlinearity coefficient on the switching action

Fig.5(d) also shows that an increase in the nonlinearity coefficient n_2 makes the grating switch for a smaller input intensity.

V. DUFFING MODEL OF NONLINEARITY AND COMPARISON WITH THE KERR MODEL

All the models described in the previous sections are developed for either purely dispersive or nonlinear materials. In many modern applications optical waves propagate through materials that exhibit both dispersive and nonlinear behaviour, and therefore a more general model is desired. However, if the simple stub technique is used to simulate both, for example Lorenzian dispersive material and Kerr nonlinearity, then the TLM model becomes unstable. It has been suggested that the Duffing model [12] can be used to simulate nonlinear dispersive dielectrics. The Duffing model [12] represents the nonlinearity as a polarisation-driven phenomenon and thus is more physically realistic than the Kerr model. This model has been previously used to simulate nonlinear Lorentz materials [7] and to simulate chaotic dynamics in nonlinear dispersive dielectric materials [13]. Both models have been implemented using a *Z*-transform technique [7], which has been shown to be a stable method that can be used to model complex materials properties [6, 7, 13].

In this section we compare results obtained using TLM implementations of the Kerr and Duffing nonlinearity models, basing the simulations around an all-optical limiter device. The all-optical limiter will first be modelled using the Kerr model for nonlinearity and results compared with those given in [14]. The equivalent Duffing model for the all-optical limiter will then be derived for both non-dispersive and dispersive case.

The Duffing polarisation equation is given by:

$$\frac{\partial^2 P(t)}{\partial t^2} + 2\delta \frac{\partial P(t)}{\partial t} + \omega_0^2 (1 + \alpha P^2(t)) P(t) = \varepsilon_0 \Delta\chi_e \omega_0^2 E(t) \qquad (7)$$

Here, P is the polarisation, E is the electric field, α is the nonlinearity coefficient, ω_0 is the resonant frequency and $\Delta\chi_e$ is the susceptibility contrast. For the non-dispersive nonlinear case, (7) reduces to:

$$P + \alpha P^3 = \varepsilon_0 \Delta\chi_e E \qquad (8)$$

The corresponding Kerr polarisation equation is

$$P = \varepsilon_0 (n_0^2 - 1) E + \varepsilon_0 2 n_0 n_2 I E \qquad (9)$$

where n_0 is the linear index, n_2 is the nonlinearity coefficient and I is the intensity of light. To ensure that both the Kerr and Duffing models have similar responses for small signals, the relation between the Kerr and Duffing models is derived as:

$$\alpha = -\frac{2 n_0 n_2}{\varepsilon_0^2 \Delta\chi_e^3 2\eta_0} \qquad (10)$$

where η_0 is the characteristic impedance of free space. The polarisation behaviour w.r.t. electric field for positive and

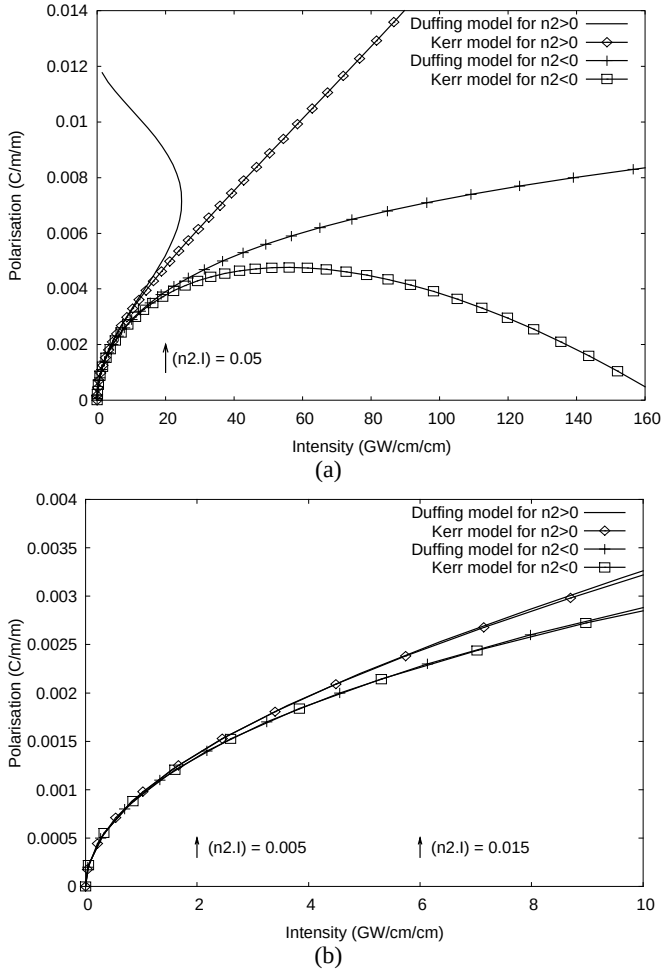

Fig. 6. (a) The polarisation behaviour of the Kerr and Duffing models obtained from the polarisation equations, (b) The small signal range enlarged

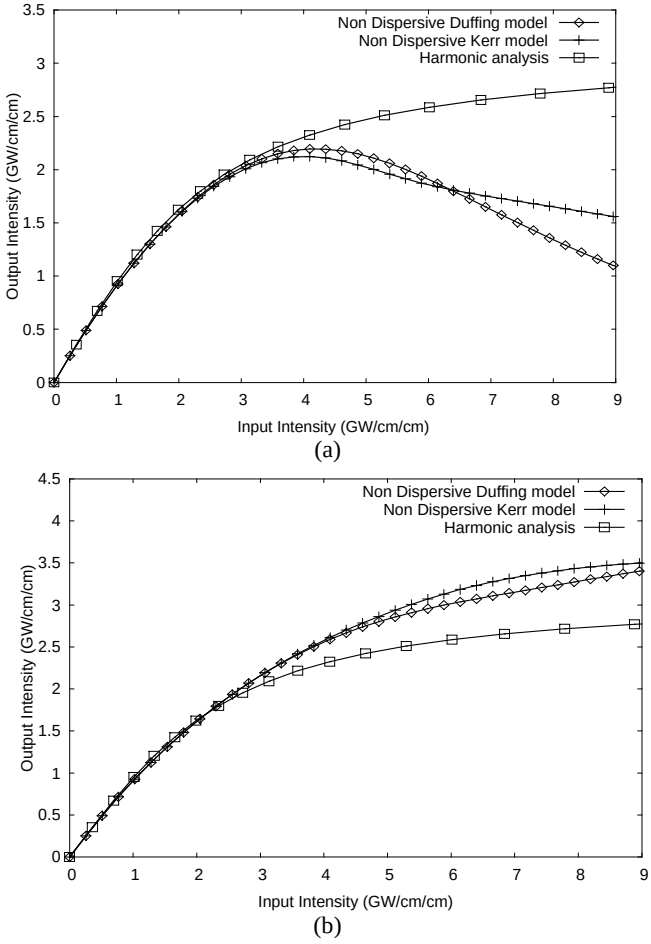

Fig.7. (a) Kerr and Duffing models for nonlinear non-dispersive grating considering only the fundamental frequency at the output, (b) including higher harmonics generated. Also shown is the result of an harmonic analysis [14].

negative Kerr nonlinearity using Kerr and Duffing models is plotted using eqs.(8,9) in Fig.6(a,b). The parameters are n_0 = 1.5, $|n_2|$ = 2.5 x 10^{-16} and $\Delta\chi_e$ = 1.25. The equivalence between the Kerr and Duffing models is valid for small input signals as is detailed in Fig.6(b). Fig.6(a) also shows the bistable nature of the Kerr model for negative nonlinearity and Duffing model for positive Kerr nonlinearity. This will be discussed further in section VI.

Having established the material models, an optical limiter structure is simulated. This is a grating similar to that studied in section IV, but with a different refractive index profile. The alternate layers in the present case have the same linear refractive index of 1.5. In addition, the alternate layers have positive and negative Kerr nonlinearity coefficients, such that the index of alternate layers for the Kerr model is given by

$$n = n_0 \pm n_2 I \tag{11}$$

where n_2 in this case is now 2.5 x 10^{-16} m^2/W. Such a grating passes a low intensity signal at the Bragg frequency through it, without significant reflection. However, for larger intensities, an instantaneous stopband begins to appear, whose centre frequency remains fixed at the Bragg frequency and whose width increases with increasing intensity. This results in a decreased transmittance of the signal, thus limiting the output intensity [14].

Fig.7(a) shows a plot of the input and output intensities of the grating consisting of a total of 150 layers simulated using both the Kerr and Duffing models. A TLM cell size Δl is chosen such that a single wavelength in material at the Bragg frequency corresponds to $48\Delta l$. A total of 1830 cells are taken, in which the grating extends from the 25^{th} to the 1824^{th} cell, and the remaining cells represent a linear material. In this simulation only the fundamental harmonic is extracted. The limiting behaviour of the structure can be observed but it does not agree well with the harmonic analysis [14] result for higher input intensities. Fig.7(b) shows the effect of including the higher order harmonics which are generated at higher input intensities in the output intensity calculations. It can be seen that the inclusion of higher harmonics improves the agreement between the TLM results and the harmonic analysis at higher input intensities. Harmonic analysis is an approximate spectral method and consequently the agreement with the TLM results is not expected to be exact especially at high intensities where nonlinear effects are more significant.

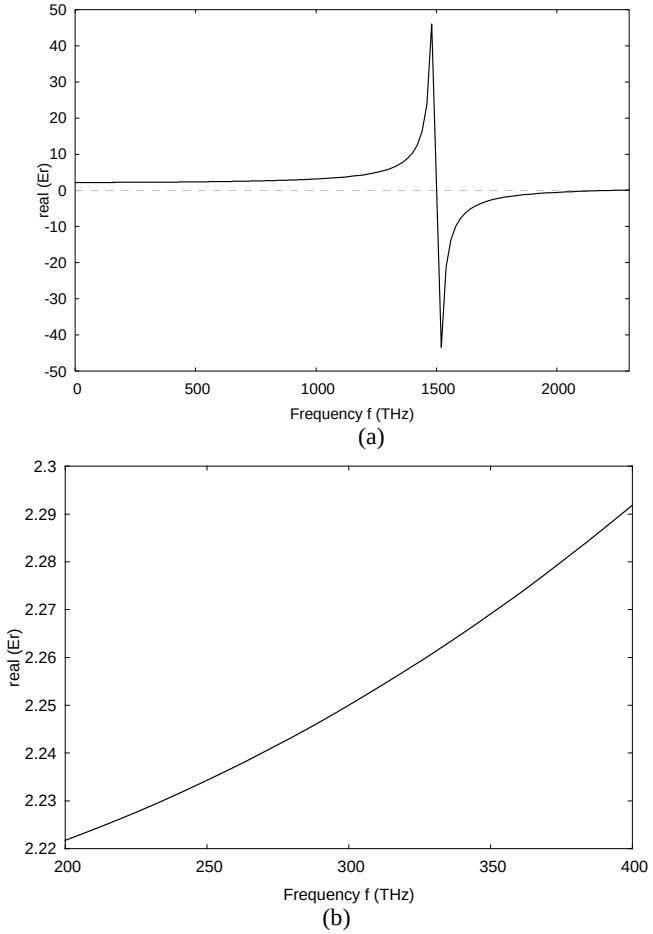

Fig.8. (a) The dispersion characteristic of the real part of dielectric permittivity, and (b) magnified region of the dispersion curve around 300 THz.

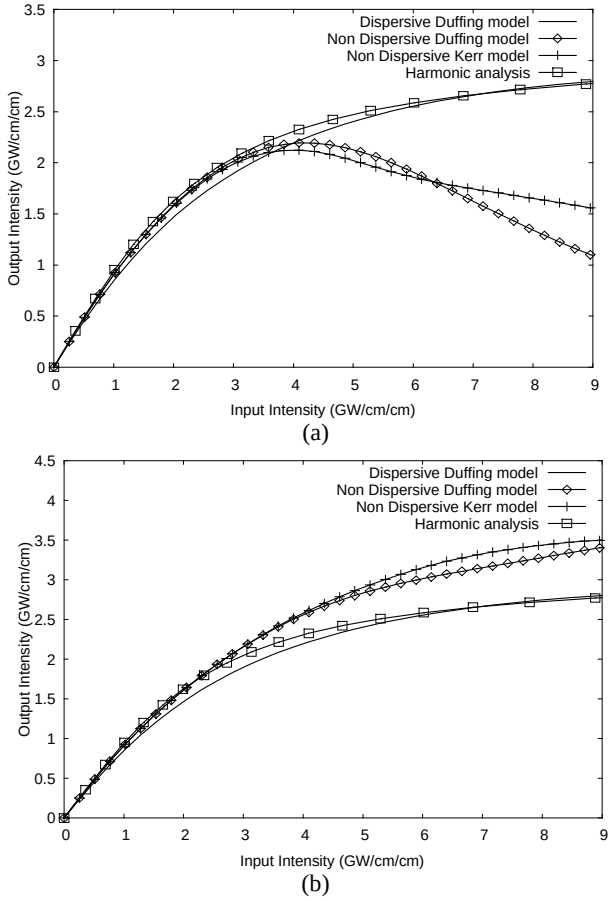

Fig.9. Comparison of the dispersive Duffing model with the non-dispresive Kerr and Duffing models and results obtained using harmonic analysis when, (a) only the principal harmonic is included and (b) higher order harmonics are included.

Simulations are now carried out for a limiter consisting of a nonlinear dispersive material (Eq. (7)). The basic structure of the grating is the same as that of Fig.7, but the model now accounts for the dispersion of the susceptibility. The parameters for the material are $\omega_0 = 2\pi$ x 1500 THz, which lies in the infrared region, and $\delta = 0.001$ x ω_0. The value of α is unchanged from Eq. (10). The value of $\Delta\chi_e$ used is 1.20 instead of 1.25 to ensure that the permittivity at the operating frequency of 300 THz is 2.25, which corresponds to an index of 1.5. This is necessary to ensure that all layers in the grating have a thickness equal to a quarter-wavelengthat 300 THz. The dispersion characteristic for the real part of dielectric constant is shown in Fig.8(a) and Fig.8(b) expands the region around 300 THz.

Fig.9 shows simulation results for the optical limiter using the full Duffing model and compares it with results obtained using the harmonic analysis and the non-dispersive Duffing and Kerr models. The results from the non-dispersive Duffing and Kerr models in Fig.9(a) are those obtained by extracting only the fundamental harmonic and in Fig.9(b) by including the higher order harmonics. It can be seen that unlike the non-dispersive Kerr and Duffing models that are significantly affected by the inclusion of higher order harmonics, the full Duffing model remains unchanged. The good agreement with harmonic analysis [14] is due to the fact that Duffing model includes out of band loss and thus naturally attenuates higher order harmonics, which is often the case in practice.

VI. Bistability of the Kerr and Duffing Model

The Kerr model for negative nonlinearity and Duffing model for positive Kerr nonlinearity exhibit bistable behaviour, as can be seen from Fig.6(a). This results in numerical instability for high input intensities. The way the instabilities are exhibited in the TLM implementation of the models is here explained for the case of the Kerr model for negative nonlinearity.

The nonlinear polarisation equations for the Kerr model are implemented numerically in the TLM, and the roots of the nonlinear equations are found using a Newton-Raphson method by which the new refined root R_{new} and the previous root R_{old} are related by:

$$R_{new} \leftarrow R_{old} - f/f' \tag{12}$$

Here the function f' is the derivative of the function f which for the Kerr model is obtained as in [11].

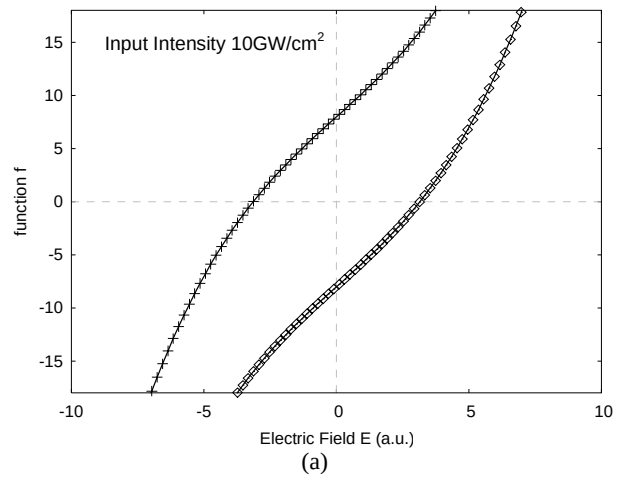

(a)

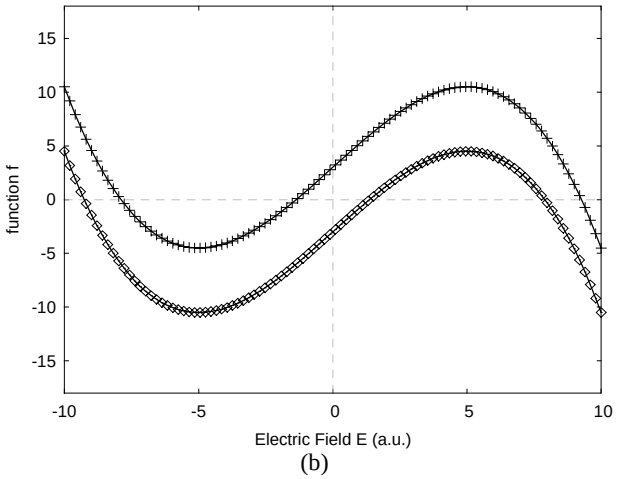

(b)

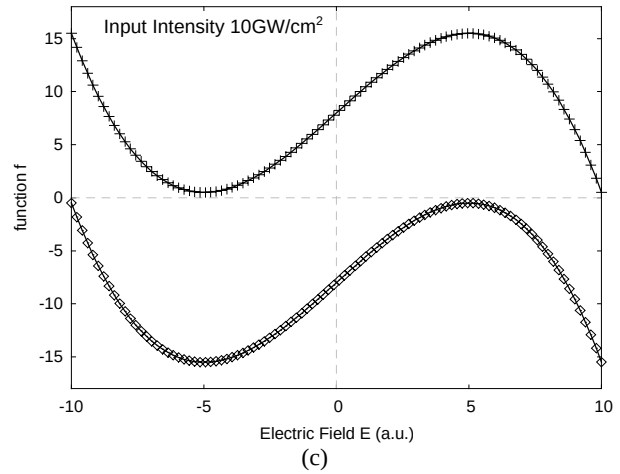

(c)

Fig.10. The behaviour of the function *f* with respect to electric field for different input intensities for (a) the positive Kerr material (b) the negative Kerr material and (c) function *f* for two extreme cases of high input intensities.

The possible variation of the function *f* with respect to the electric field at the particular node is plotted for different values of the input intensities in Fig.10(a,b). Fig.10(a) shows the typical behaviour of function *f* for the Kerr model for positive nonlinear materials. Two curves for input intensity of 10GW/cm^2 in Fig.10(a) depict the behaviour of the forcing function at two different nodes. It can be seen that a change in input intensity shifts the curve *f* up or down thus always giving a single root and resulting in a stable model. However, in the case of the Kerr model for negative nonlinear materials, and small input intensities, the curve has a different shape, with three potential zeros, as shown in Fig.10(b). The physically consistent solution is the one yielding the lowest value for the electric field. In the case of low input intensities it is possible to select the lowest solution and thus ensure stability. However, for high input intensities the curve shifts significantly up or down, as shown in Fig.10(c). It can be shown that the single zero for the electric field that can be obtained in these extreme cases, when replaced in the eq.(11), results in the dielectric constant lower than unity which is not physical. The behaviour of the function *f* for this case is shown in Fig.10(c) for a high input intensity of 10 GW/cm^2. Numerically both cases shown in Fig.10(c) can occur. These instabilities are of similar nature for the Duffing model for the positive Kerr nonlinearity, as indeed observed in Fig.6(a). It is emphasized here that these numerical instabilities are consequences of the bistable properties of the Kerr or Duffing models and are not characteristic to the TLM method.

VII. CONCLUSIONS

This paper has presented different TLM models for dispersive and nonlinear materials. Two models for modelling nonlinear materials, the Kerr model and the Duffing model have been directly related and results compared for the case of nonlinear non-dispersive materials. The two models agree very well for the case of small signals. Both models, when applied to model particular nonlinear material can exhibit bistability. The full Duffing model can be used to simulate nonlinear dispersive materials and has been applied in this paper to the structure of the optical limiter. The results obtained using the Duffing model agree very well with those obtained using harmonic analysis due to the out of band loss that is intrinsically incorporated into the Duffing model.

REFERENCES

[1] N. Bloembergen, *Nonlinear optics: past, present, and future.* IEEE Journal on Selected Topics in Quantum Electronics, 2000. **6**(6): p. 876-880.

[2] A. Suryanto, E.V. Groesen, M. Hammer, and H.J.W.M. Hoekstra, *A finite element scheme to study the nonlinear optical response of a finite grating without and with defect.* Optical and Quantum Electronics, 2003. **35**: p. 313-332.

[3] D. Pelinovsky, J. Sears, L. Brzozowski, and E.H. Sargent, *Stable all-optical limiting in nonlinear periodic structures. I.Analysis.* Opt.Soc.Am.B, 2002. **19**(1): p. 43-53.

[4] N.M. Litchinitser, B.J. Eggleton, and G.P. Agrawal, *Dispersion of cascaded fibre gratings in WDM lightwave systems.* Journal of Lightwave Technology, 1998. **16**(8): p. 1523-1529.

[5] P. Tran, *Optical limiting and switching of short pulses by use of a nonlinear photonic bandgap with a defect.* Opt. Soc. Am. B, 1997. **14**(10): p. 2589-2595.

[6] J. Paul, C. Christopoulos, and D.W.P. Thomas, *Generalized Material Models in TLM - Part I : Materials With Frequency-Dependent Properties.* IEEE Trans., Antennas and Prop., 1999. **47**(10): p. 1528-1534.
[7] J. Paul, C. Christopoulos, and D.W.P. Thomas, *Generalized Material Models in TLM - Part 3 : Materials With Nonlinear Properties.* IEEE Trans., Antennas and Prop., 2002. **50**(7): p. 997-1004.
[8] A. Taflove and S. Hagness, *Computational Electrodynamics : The Finite-Difference Time-Domain Method*. 2000: Artech House.
[9] C. Christopoulos, *The transmission-line modeling method: TLM*. 1995, Piscataway, NJ: IEEE Press.
[10] H. Xiao and K.E. Oughstun, *Hybrid Numerical-Asymptotic Code for Dispersive-Pulse Propagation Calculations.* J. Opt. Soc. Am. A, 1998. **15**(5): p. 1256-1267.
[11] V. Janyani, A. Vukovic, T.M. Benson, and P. Sewell. *Modelling of Non-Linear Optical Materials Using the TLM Method*. in *6th International Conference on Applied Electromagnetics*. 2003. Nis, Yugoslavia: p. 143-146.
[12] M. Yamane and Y. Asahara, *Glasses for Photonics*. 2000, Cambridge: Cambridge University Press.
[13] J. Paul, C. Christopoulos, and D.W.P. Thomas. *Time-Domain Simulation of Chaotic Dynamics in Nonlinear Frequency-Dependent Dielectric Materials*. in *(to appear in) The 20th Annual Review of Progress in Applied Computational Electromagnetics (ACES 2004)*. 2004. Syracuse University, NY
[14] L. Brozozowski and E.H. Sargent, *Optical Signal Processing Using Nonlinear Distributed Feedback Structures.* IEEE J. Q. E., 2000. **36**(5): p. 550-555

.